Surface barrier in metals: A new model with application to W(001)

R. O. Jones
Institut für Festkörperforschung der Kernforschungsanlage Jülich, D-5170 Jülich, Federal Republic of Germany

P. J. Jennings
School of Mathematical and Physical Sciences, Murdoch University, Murdoch, Western Australia 6150, Australia

O. Jepsen
Max-Planck-Institut für Festkörperforschung, D-7000 Stuttgart 80, Federal Republic of Germany
(Received 5 December 1983)

A new model of the surface barrier at a metal surface is presented. It is one dimensional, has two adjustable parameters (z_0, the location of the image plane, and λ, which determines the length scale of the transition from vacuum to bulk), and its form is suggested by the results of self-consistent electronic-structure calculations for a five-layer film of W(001) described here. The optimum form for electrons with incident energies below 10 eV is determined by comparison with available low-energy-electron-diffraction data from W(001).

I. INTRODUCTION

Charge-transfer processes occur in many branches of surface science, such as Schottky-barrier transmission and thermionic and field emission. Particularly important are spectroscopic methods which use charged particles, examples being photoemission and the scattering of low-energy electrons and positrons. Although not all these techniques are equally sensitive to the form of the potential barrier at the surface, a detailed knowledge is usually essential for a complete analysis of such processes.

In classical electrostatics, the form of the potential barrier outside the surface of a perfect conductor can be found by solving Laplace's equation using the method of images. The classical image barrier for a charge q at point z is as follows:

$$V(z)=\frac{q^2}{2z}, \quad z<0 , \tag{1}$$

where the metal occupies the half-space $z>0$. Unless otherwise stated, we use rydberg atomic units throughout.

There are several problems associated with the use of Eq. (1) for describing surface processes such as those listed above. The divergence at $z=0$ is unphysical. The potential should go smoothly to its bulk value, a modification which is commonly referred to as image-potential "saturation." A more realistic description of the metal surface could also result in the modification of the asymptotic form, for example, a shift in the image plane.

A quantum-mechanical description of the surface-potential barrier experienced by an electron was given by Bardeen.[1] He performed a one-dimensional approximate Hartree-Fock analysis of a jellium model and showed that the barrier arose mainly from exchange and correlation effects. If the potential inside the metal was assumed to be constant, the image form (1) should be asymptotically correct, but substantial deviations were noticeable within $(2-3)a_0$ from a jellium surface with an electron density appropriate to that of Na. Shortly thereafter MacColl[2] calculated the surface-barrier reflectivity for a one-dimensional potential of image form cutoff at a constant value V_0.

The problem has been studied by numerous authors since that time. Of particular interest for the present work was the observation by Cutler and Davis[3] that the long-range ($z \lesssim -10a_0$) behavior of the potential of Bardeen could be approximated by the following:

$$V(z)=\frac{q^2}{2z}(1-e^{\lambda z}), \quad z \lesssim -10a_0 , \tag{2}$$

where the damping factor λ describes saturation effects. Further insight into the form of the static potential barrier resulted from self-consistent calculations for jellium surfaces using a local approximation for exchange and correlation.[4] This approximation leads to an incorrect exponential decay in the potential far outside the surface, and, since the calculations focus on the effective potential "felt" by occupied states, they do not provide a reliable estimate of the potential appropriate for more energetic electrons. The results should nevertheless give a reasonable picture of the transition from bulk to vacuum, and an example is given in Fig. 1 for a jellium model with $r_s=2$. For a jellium model, the asymptotic form of the potential outside the surface can be related to surface properties by the observation[5] that

$$V(z)=\frac{q^2}{2(z-z_0)}, \quad z \to -\infty \tag{3}$$

where z_0 is the center of mass of the induced charge distribution (relative to the edge of the positive background). The position of the image plane z_0 depends on the method of calculation,[6] but lies $0.5a_0-1.5a_0$ outside the edge of the jellium background for metallic densities. The image-plane location is weakly dependent on the screening

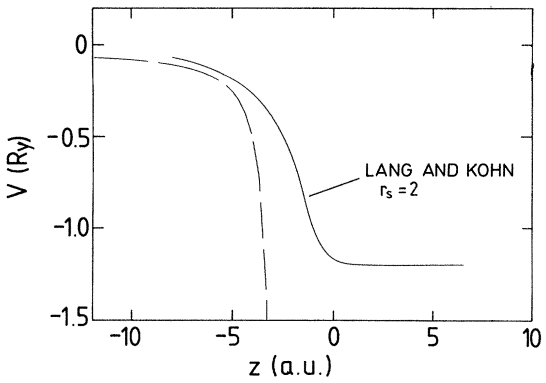

FIG. 1. Effective potential at jellium surface for $r_s=2$, plotted from results of Ref. 4. The origin is located $1.5a_0$ inside the jellium edge. Also shown (dashed curve) is the classical image potential relative to an image plane at $z_0=-3.1a_0$ (Ref. 5).

radius in the metal, lying closer to the jellium edge as r_s increases.

The above arguments then suggest a surface barrier with an asymptotic form (3) and a transition to the bulk potential similar to that of Fig. 1. However, it was already evident in the work of Bardeen[1] that no single barrier can be satisfactory for electrons of all velocities and dynamical corrections to the image potential have been discussed by several authors. Harris and Jones,[7] for example, performed detailed calculations for a simplified model of a metal surface and showed that velocity-dependent effects could be understood in terms of the interaction between the moving charge and its spatially retarded image.

With the improvement of electron scattering measurements, particularly low-energy electron diffraction (LEED), it has become essential for theorists to use increasingly refined barrier models. Early work used variants of the step barrier, which consists simply of a discontinuity in the potential at the plane $z=a$:

$$V(z)=\begin{cases}0, & z<a\\ -U_0, & z>a\ .\end{cases} \tag{4}$$

This model is simple to treat analytically, but the sharp discontinuity leads to unphysical results. Other authors[8] have used an exponential barrier shape for the transition region,

$$V(z)=-U_0/[1+\exp(-\beta z)]\ . \tag{5}$$

This model is also straightforward to treat analytically, and it provides a rough approximation to the results of jellium calculations such as those shown in Fig. 1.

The modified image barrier, which is based on classical electrostatics, was suggested by Cutler and Gibbons,[9]

$$V(z)=\begin{cases}\dfrac{q^2}{2(z-z_0)}+\dfrac{\eta q^2}{2(z-z_0)^2}, & z<z_c\\ -U_0, & z>z_c\ .\end{cases} \tag{6}$$

This model gives generally satisfactory results in calculations of LEED fine structure[10] as well as periodic deviations from the Schottky effect in thermionic emission.[9] A modification of this form, with an interpolation region between the two in Eq. (6), has been used by Rundgren and Malmström[11] and recently by Hall *et al.*[12] to interpret high-resolution electron scattering data.

Recently, Dietz *et al.*[13] showed that improved agreement with LEED fine-structure measurements could be obtained by using a barrier in which a linear interpolation between vacuum and bulk regions is used,

$$V(z)=\begin{cases}\dfrac{q^2}{2(z-z_0)}, & z<z_1\\ -U_1-\dfrac{q^2 z}{2(z_1-z_0)}, & z_1<z<0\\ -U_0, & z>0,\end{cases} \tag{7}$$

with two adjustable parameters U_1 (the step height at $z=0$) and z_0 (the image-plane location). The barrier was used successfully to reproduce experimental data[13] on Cu(001), and recently we showed[14] that a minor modification enabled the presentation of a consistent picture of available high-resolution and spin-polarized LEED measurements for W(001). In particular, it was possible to separate unambiguously barrier scattering effects from spin-dependent and Bragg features. An additional interesting feature of this work was the discovery that several barriers provided equally good fits of individual intensity energy curves. This is a consequence of the interference origin of the fine structure and will be discussed further below.

In spite of the satisfactory results obtained using the model barrier (7), the linear interpolation used can only be approximate, and the increasing availability of high-resolution data means that better discrimination between barrier models is becoming possible. It is the aim of this paper to describe a model of the surface-barrier potential that is one dimensional, has two free parameters, and should be useful in other contexts. The transition from the shifted image form (7) to the bulk potential is suggested by self-consistent density-functional calculations carried out for a five-layer W(001) film. These calculations are described in Sec. II. In Sec. III the potential is averaged parallel to the surface and the results suggest a simple, physical parametrization of the barrier. The parameters are optimized for W(001) in Sec. IV by comparison with experimental data on W(001) (energies 0—10 eV, angle of incidence θ up to 48°). The present state of the barrier parametrization question and possible future modifications are discussed in Sec. V, and our conclusions are listed in Sec. VI.

II. SELF-CONSISTENT FILM CALCULATIONS—W(001)

In this section, we present results of a self-consistent energy-band calculation for a five-layer W(001) film.[15] For the purpose of this discussion, we assume that the potential for the central layer is representative of the bulk. The potential for the film geometry of Fig. 2 was deter-

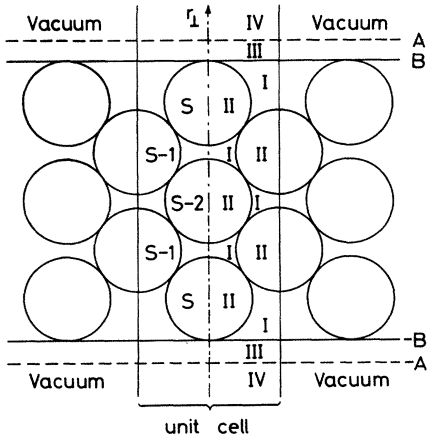

FIG. 2. (110) cross section of five-layer W(001) film showing separation of space into different regions.

mined by solving the Schrödinger-like density-functional equations using a local approximation for exchange and correlation.[16] Details of the linear-augmented-plane-wave (LAPW) method used for the construction of the charge density and potential are given in Refs. 17 and 18, respectively. The LAPW basis functions and the charge density constructed from them are continuous with continuous derivatives at the boundaries of all regions in Fig. 2.

The valence charge density can be represented as a plane-wave expansion extending over regions I, II, and III, and a remainder which is approximated by its muffin-tin component in regions II, III, and IV. With a frozen-core approximation, it is relatively easy to calculate the potential components and to express them in the same form as the charge density,[18] i.e.,

$$V(\vec{r})=V_{\mathrm{MT}}(\vec{r})+\sum_{\vec{G}} e^{i\vec{G}\cdot\vec{r}}V(\vec{G}) + \sum_{\vec{G}_{\parallel}} e^{i\vec{G}_{\parallel}\cdot\vec{r}_{\parallel}}\cosh(G_{\parallel}r_{\perp})b(\vec{G}_{\parallel}) \, . \tag{8}$$

The muffin-tin potential V_{MT} is constant in region I, spherically symmetric in region II, and planar symmetric in regions III and IV. The non-muffin-tin part enters only via the plane-wave expansion and it can easily be included as plane-wave matrix elements throughout the A slab. Outside this slab, the corrugation of the potential

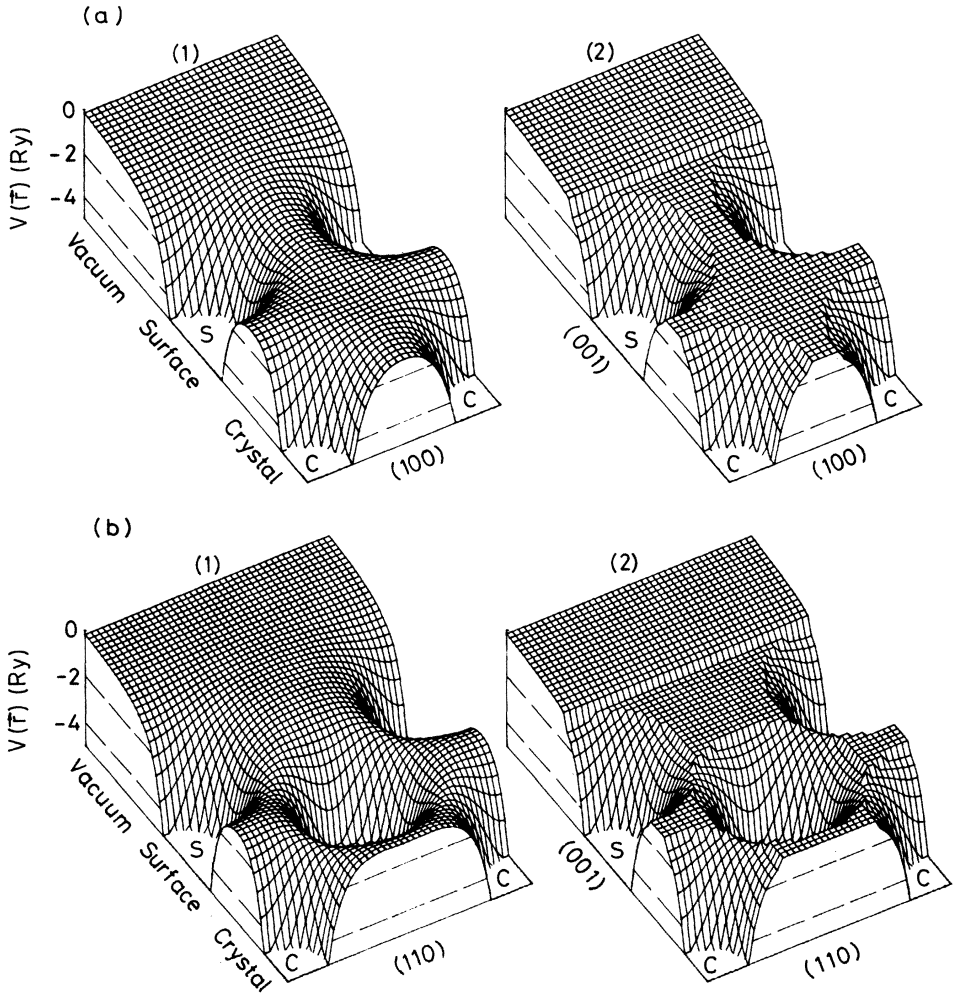

FIG. 3. Variation of the self-consistent potential for W(001) film in (a) (100) and (b) (110) planes perpendicular to the surface and containing the surface atom (S), the subsurface atom and the atom in the central layer (C). Part (1) is the full potential and part (2) is the muffin-tin contribution.

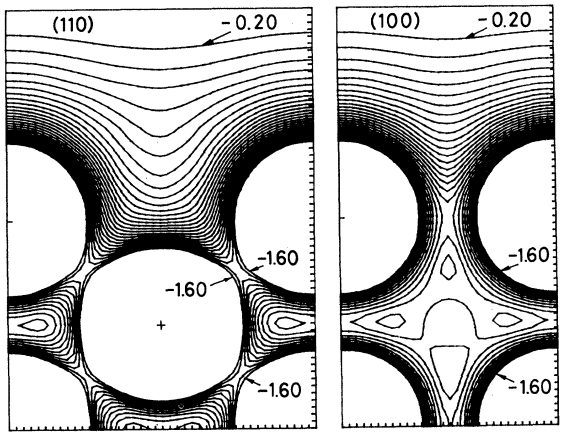

FIG. 4. Contour plot of the self-consistent potential in (110) and (100) planes perpendicular to the W(001) film. The contours are marked in rydberg units and the interval is 0.05 Ry.

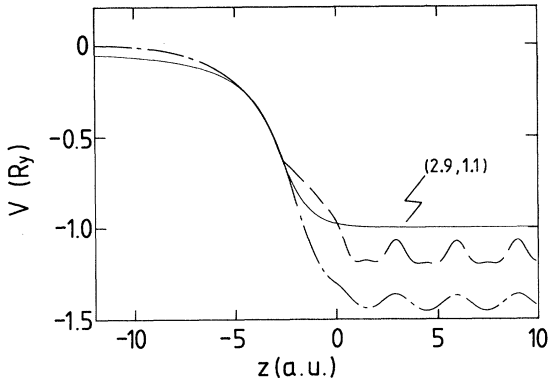

FIG. 5. Self-consistent film potential averaged parallel to the surface (dashed-dotted curve) and the average excluding regions II of Fig. 2 (dashed curve). The slope discontinuities in the latter are due to these exclusions. Also shown is the model barrier Eq. (9) with $z_0=-2.9a_0$, $\lambda=1.1a_0^{-1}$ (solid curve).

parallel to the film is neglected.

These calculations were carried out for an unreconstructed bulk geometry and included more than 50 basis functions per atom, leading to mRy accuracy in the eigenvalues. Integrations over the two-dimensional Brillouin zone were performed using the linear triangular method[17] with 28 points in the irreducible part of the zone. The self-consistent potential should have the same accuracy as the eigenvalues. In spite of the known shortcomings of the local approximation for the exchange-correlation potential, the calculated work function (4.3 eV) is in good agreement with the experimental value of 4.6 eV.[19]

The self-consistent potential for the three outermost layers is shown in Figs. 3 and 4 and has some interesting features. In particular, Fig. 3 shows that the muffin-tin term is the dominant contribution to the potential. The contour plots of Fig. 4 show, however, that the potential has a distinctly three-dimensional character. We shall return to this point in Sec. V.

III. SURFACE-BARRIER MODEL

The barrier models discussed in Sec. I are all one-dimensional. They can be compared with the results of Sec. II by averaging the latter parallel to the surface. For the potential representation in Eq. (7), this can be performed analytically in terms of the potential parameters $V(\vec{G})$ and $b(\vec{G})$ for planes of integrations both with and without the circular intersections with the muffin-tin spheres. Results for both these averages are shown in Fig. 5. The average of the potential in region I (-0.965 Ry) is different from the bulk values obtained by the two methods of averaging. The inner potential U_0 is, however, usually determined by matching calculated and experimental features, such as peak positions or thresholds.

Although the density-functional formalism is the basis of both the jellium and tungsten calculations, the similarity between the potential variations in Figs. 1 and 5 is remarkable. The form of the results leads us to propose the following barrier model:

$$V(z)=\begin{cases}\dfrac{1}{2(z-z_0)}(1-e^{\lambda(z-z_0)}), & z<z_0\\[2ex] \dfrac{-U_0}{Ae^{-\beta(z-z_0)}+1}, & z>z_0\ ,\end{cases} \tag{9}$$

where the constants A and β are determined by matching $V(z)$ and its derivative at the image plane $z=z_0$. This leads to

$$\beta=U_0/A\ ,\qquad A=-1+2U_0/\lambda\ . \tag{10}$$

Far outside the surface, the barrier has the form suggested by Cutler and Davis [Eq. (2) above], but with a shift in the image plane in line with the considerations of Sec. I. The quantity λ determines the range of transition from the vacuum potential to its value in the bulk. It has a simple physical interpretation, since $-\lambda/2$ is the value of the potential at the image plane.

In Fig. 5 we also show the model barrier of Eq. (9) with the parameters $z_0=-2.9a_0$, $\lambda=1.1a_0^{-1}$, and $U_0=1$ Ry. It is clear that the form (9) provides a much better representation of the potential in the transition region than the linear interpolation used previously. Barriers corresponding to nearby points in the (z_0,λ) plane lead to qualitatively similar barriers, particularly if the image plane is moved further from the surface with a corresponding increase in the transition range $1/\lambda$. For barriers corresponding to a narrow band of values in the (z_0,λ) plane, we may then expect similar LEED intensity curves.

The parameters obtained from the fit to the potential from the layer calculations are appropriate for occupied states well below the energies of incident electrons. They should, however, provide a valuable guide to the barrier parameters for electrons above the vacuum level. In analyzing LEED experiments, we expect U_0 to decrease with increasing energy.[20] Furthermore, dynamical effects could lead to changes in z_0 and λ, since electrons moving towards or parallel to the surface should have a weaker in-

teraction with it than in the case of a stationary electron.[7] Since U_0 can be determined with some precision by comparison with experiment, we believe that the model barrier (9), with two physically meaningful adjustable parameters, should be a useful starting point for surface-barrier effects in general. In the following section, we analyze published data on W(001).

IV. DETERMINATION OF BARRIER PARAMETERS FOR W(001)

The method used to calculate the diffracted electron intensities is described in detail in Ref. 14. The scattering properties of the semi-infinite crystal are described by the layer multiple-scattering method, which leads to the total amplitude reflection matrix

$$\underline{R}_T^{-+}=\underline{r}^{-+}+\underline{t}^{--}\underline{R}^{-+}(\underline{1}-\underline{r}^{+-}\underline{R}^{-+})^{-1}\underline{t}^{++} . \quad (11)$$

$\underline{R}$ describes the scattering properties of the substrate, $\underline{r}$ and $\underline{t}$ are reflection and transition matrices for the surface barrier, and $\underline{r}^{-+}$, for example, denotes the scattering of an electron moving in the direction of $z>0$ into the $z<0$ direction. Although the matrices $\underline{r}$ and $\underline{t}$ are found by integration into the bulk, it is important to note that the *phases* depend on the position of the barrier z_0. The strength of inelastic scattering allows us to express the inverse matrix as a series and to truncate the series to include only "double-diffraction" terms.[14] In these calculations, we have made minor changes which lead to more accurate results in the immediate neighborhood of thresholds.

The experimental data are the same as used in Ref. 14. They comprise high-resolution (15-meV) reflectivities for angle of incidence $\theta=48°$ (Ref. 21) and spin-polarized intensities for $15°<\theta<43°$.[22] The incident energies E are between 0 and 10 eV and we have assumed that $U_0=1$ Ry over this range. The energy dependence of U_0 should be considered for larger energy ranges.

Inelastic scattering processes play an important role in determining the reflected intensities. In our earlier work[14] we used an energy-dependent imaginary potential to describe the bulk damping, with a barrier damping $V_{\rm im}$ given by

$$V_{\rm im}=0.1\exp(-0.1z^2) . \quad (12)$$

In this work, we use a bulk damping

$$V_{\rm im}^{\rm bulk}(E)=V_0(1+e/\phi)^{1.7} , \quad (13)$$

with $V_0=0.1$ Ry and $\phi=5$ eV. This form was suggested by McRae and Caldwell,[23] following electron-reflectivity measurements on other transition metals, and produces relatively minor changes in the calculated peak positions. More significant is our use of the barrier damping

$$V_{\rm im}(E)=\alpha V_{\rm im}^{\rm bulk}(E)\exp(-\beta|z|) . \quad (14)$$

The surface-barrier damping is then proportional to the bulk damping [Eq. (13)], is centered on the outermost atomic plane, and decays *exponentially* into both bulk and vacuum. For energies above 10 eV, the damping is considerably stronger than that in Ref. 14, which we have found to be necessary to describe high-resolution data in this range.[24] For energies below 10 eV, however, the intensities depend most sensitively on the barrier parameters z_0 and λ, and we have used the scaling factor $\alpha=1$ and the exponent $\beta=0.2a_0^{-1}$ throughout.

As in our earlier work, we have used the high-resolution data at 48° to locate the regions in the space of barrier parameters (z_0,λ) which reproduce the reflectivity extrema accurately. In Ref. 14 we found that saturated image barriers centered at $-7a_0$, $-3.3a_0$, and 0 gave equally good fits to the peak positions for $\theta=48°$ and a similar effect was found in the present calculations. The interference nature of the mechanism means that phase changes near 2π in the matrices $\underline{r}$ and $\underline{t}$ [Eq. (10)] lead to similar calculated intensities. Over the restricted energy range considered here, this is possible by changing either the position of the image plane or by large changes in λ. The film calculations show, however, that not all regions of (z_0,λ) space are physically reasonable. The value of z_0 should not be too different from its static value, and "saturation" effects due to the weaker interaction felt by an electron moving towards or parallel to the surface rule out λ values significantly greater than the fit to the film potential ($\lambda=1.1a_0^{-1}$).

These considerations reduce the number of barriers yielding satisfactory agreement with the fine structure in the 48° data to a narrow region of (z_0,λ) space from $(-2.6,1.1)$ and $(-3.3,0.7)$. As noted in Sec. III, barriers along such a line are similar and even a resolution of 15 meV does not permit a clear distinction between them. In Fig. 6 we show that the calculated fine structure for the barrier $(-3.1,0.8)$ compares very well with the experimental measurements.[21] As noted in Ref. 14, spin-dependent effects are not pronounced for these energies and incident angles. The energy zero in the experimental curve has been moved upwards by 0.13 eV and the energy of the

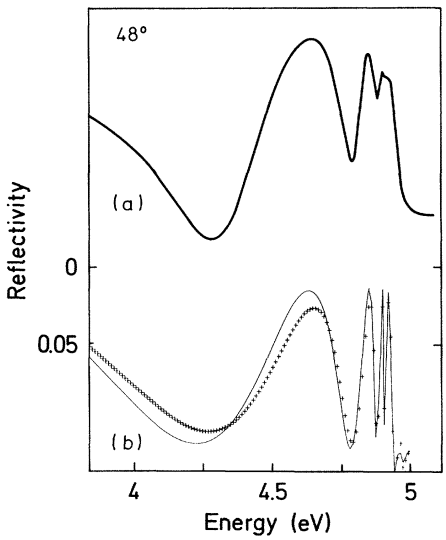

FIG. 6. Comparison between calculated and experimental fine structure for $\theta=48°$. (a) Experiment, after Ref. 21. The energy zero has been shifted upwards by 0.13 eV. (b) Calculated spin-polarized intensities for barrier with $z_0=-3.1a_0$, $\lambda=0.8a_0^{-1}$. Solid curve, spin down; crosses, spin up. The fine-structure mesh is 0.01 eV.

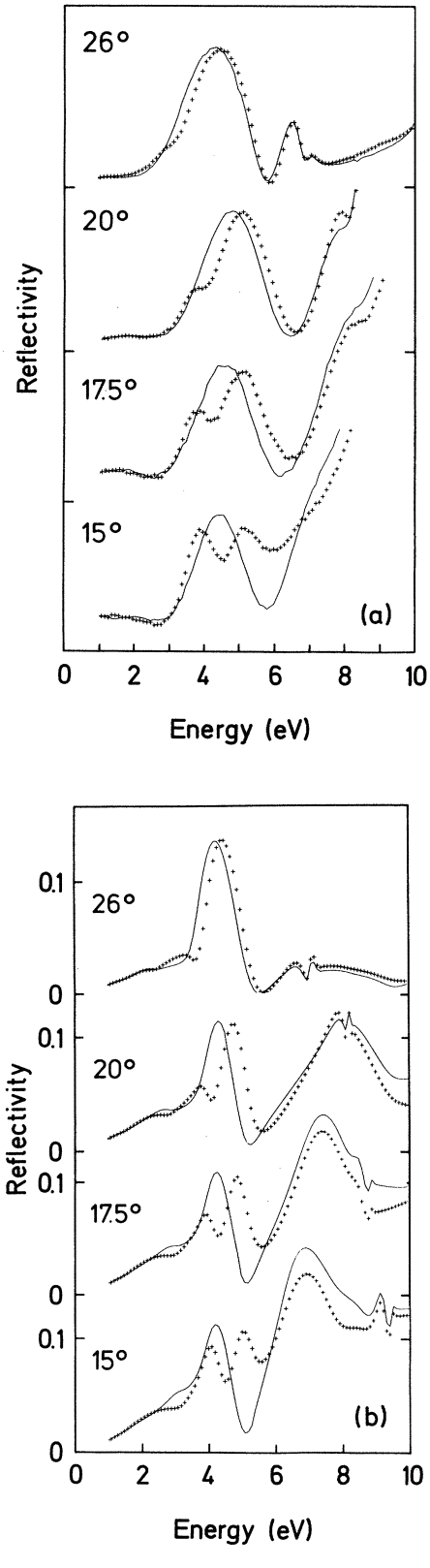

FIG. 7. Comparison between calculated and experimental spin-polarized intensities for $\theta=15°$, 17.5°, 20°, and 26°. (a) Experiment, Ref. 22. The intensities are in arbitrary units. (b) Calculated intensities for barrier with $z_0=-3.1a_0$, $\lambda=0.8a_0^{-1}$. Solid curves, spin down; crosses, spin up. The mesh is 0.1 eV.

threshold now agrees with both the calculated value and with the value found recently by Baribeau *et al.*[24] There is an additional peak near 3.5 eV (with a maximum 1.46 eV below the highest clearly resolved minimum in the data of Ref. 21) and we find that the position of this maximum is sensitive to the choice of barrier parameters. A satisfactory fit to this peak reduces the acceptable values of $(|z_0|,\lambda)$ to $(3.2\pm0.15,0.8\mp0.1)$.

In Fig. 7 we compare the measured spin-polarized intensities for $\theta=15°$, 17.5°, 20°, and 26° with those calculated using the barrier $(-3.1,0.8)$. The fine structure near threshold is not resolved in the measurement, but the striking asymmetry between spin-up and spin-down intensities is apparent. For these incident energies and angles, there is a delicate interaction between Bragg peaks, spin-dependent features, and barrier scattering effects. The agreement between theory and experiment is satisfactory.

V. DISCUSSION

The self-consistent film calculations described here show that the effective single-particle potential for occupied electrons demonstrates significant departures from the muffin-tin form assumed in almost all LEED calculations. Since threshold effects originate in the coupling of the beams by $\vec{G}$ vectors parallel to the surface, they will be affected by non-muffin-tin terms in the potential, and this is an interesting consideration for future work. It is important to note that a barrier derived from a local-density calculation is not appropriate for LEED calculations. The asymptotic form outside the crystal has an exponential rather than an inverse dependence on the distance from the surface, and the asymptotic form in the crystal has an average value which is too low for the energy range considered here (0—10 eV) and quite inappropriate for higher energies. However, the transition from vacuum to bulk should be described more satisfactorily and the results have suggested a one-dimensional model potential. The real part of this potential has two adjustable parameters, z_0, the position of the image plane, and λ, which describes the degree of barrier saturation.

The one-dimensional model [Eq. (8)] with $z_0=-3.2a_0$ and $\lambda=0.8a_0^{-1}$ provides a satisfactory fit to LEED fine-structure measurements on W(001). The relative insignificance of three-dimensional effects at this level of accuracy may be due to the high symmetry of the W(001) surface and these effects could be more important for less symmetrical surfaces, such as W(110).

This work is a refinement and extension of earlier work[10,14] and shows some interesting similarities and differences. In particular, the position of the image plane $(z_0=-3.2a_0)$ is very similar to those obtained using the modified image[10] $(-3.0a_0)$ and saturated image[14] $(-3.3a_0)$ barrier models. Although the long-range parts of these potentials are similar, the forms near the surface are quite different. In this region, the potential is complicated by dynamical and three-dimensional effects, and high-resolution and spin-polarized data, if possible in conjunction with absolute reflectivity measurements, are needed to further refine the barrier models. The interference nature of the barrier-dependent scattering means that

barriers corresponding to other regions of (z_0,λ) space lead to essentially identical peak positions. However, the optimum region given above is the only one which is qualitatively similar to the barrier in the film calculations.

This work confirms the overall picture described earlier.[14] In that analysis, we also found several barriers which described the data at $\theta=48°$ equally well, and the origin of the low-energy structure in the W(001) LEED curves—the interaction among Bragg peaks, spin-dependent features, and barrier scattering effects—is unchanged. The optimized barrier, like the saturated image barrier and the barrier determined from the film calculation, overlaps the bulk region. This is a familiar situation in LEED calculations, where the reflection and transmission matrices of each layer are usually determined separately, even if the layers overlap. In the present context, we determine the reflection and transmission matrices for the much weaker barrier scattering. Since z_0 is located outside the muffin-tins of the surface layer, the overlap is weak and the scheme we use should be reliable.

VI. CONCLUSIONS

Self-consistent electronic structure calculations have been performed for a five-layer W(001) film. The results suggest a model for the scattering potential for electrons near the surface, and an appropriate choice of parameters $(z_0=-2.9a_0,\lambda=1.1a_0^{-1})$ reproduces satisfactorily the averaged potential of the film calculations in the transition region.

The barrier model has been used to analyze measured LEED intensity curves from W(001) with the following results.

(a) With $z_0=-3.2a_0$ and $\lambda=0.8a_0^{-1}$, the model provides a satisfactory fit to both the threshold fine structure for $\theta=48°$ and to spin-polarized measurements at lower incident angles.

(b) The optimum barrier location is close to those found in earlier work using the modified image and saturated image barrier models. The degree of saturation is, as expected, greater than in the film calculations.

(c) Three-dimensional effects in the barrier are not significant for the W(001) surface at the present level of accuracy.

High-resolution and spin-polarized LEED data appear to be capable of providing a detailed picture of the scattering potential experienced by an electron near a surface. The realization of this will require the continuing close cooperation between theory and experiment, with the development of more refined calculational models and methods of obtaining data of even higher resolution. Work in these directions is continuing.

ACKNOWLEDGMENTS

We thank D. T. Pierce, J. M. Baribeau, and the late J. D. Carette for providing the original data and for correspondence.

[1]J. Bardeen, Phys. Rev. 49, 640 (1936); 58, 727 (1940).
[2]L. A. MacColl, Phys. Rev. 56, 699 (1939).
[3]P. H. Cutler and J. C. Davis, Surf. Sci. 1, 194 (1964).
[4]N. D. Lang and W. Kohn, Phys. Rev. B 1, 4555 (1970).
[5]N. D. Lang and W. Kohn, Phys. Rev. B 7, 3541 (1973).
[6]See S. Efrima, Surf. Sci. 107, 337 (1981), and references therein.
[7]J. Harris and R. O. Jones, J. Phys. C 6, 3585 (1973); 7, 3751 (1974).
[8]See, for example, I. I. Gol'dman and V. D. Krivchenkov, *Problems in Quantum Mechanics* (Pergamon, London, 1961), p. 2; R. Feder and J. Kirschner, Surf. Sci. 103, 75 (1981).
[9]P. H. Cutler and J. J. Gibbons, Phys. Rev. 111, 394 (1958).
[10]P. J. Jennings, Surf. Sci. 75, L773 (1977); P. J. Jennings and G. L. Price, *ibid.* 95, L205 (1980).
[11]J. Rundgren and G. Malmström, J. Phys. C 10, 4671 (1977).
[12]B. M. Hall, S. Y. Tong, and D. L. Mills, Phys. Rev. Lett. 50, 1277 (1983).
[13]R. E. Dietz, E. G. McRae, and R. L. Campbell, Phys. Rev. Lett. 45, 1280 (1980).
[14]P. J. Jennings and R. O. Jones, Solid State Commun. 44, 17 (1982); R. O. Jones and P. J. Jennings, Phys. Rev. B 27, 4702 (1983).
[15]Further details are given in O. Jepsen and J. W. Wilkins (unpublished).
[16]U. von Barth and L. Hedin, J. Phys. C 5, 1629 (1972).
[17]O. Jepsen, J. Madsen, and O. K. Andersen, Phys. Rev. B 18, 605 (1978); O. K. Andersen, *ibid.* 12, 3060 (1975).
[18]O. Jepsen, J. Madsen, and O. K. Andersen, Phys. Rev. B 26, 2790 (1982). Similar self-consistent calculations have been performed for an unreconstructed seven-layer W(001) film by M. Posternak, H. Krakauer, A. J. Freeman, and D. D. Koelling, Phys. Rev. B 21, 5601 (1980). Although these authors neglected nonspherical potential terms in the muffin tins, the overall agreement between the two calculations is good. See also M. Posternak, H. Krakauer, and A. J. Freeman, Phys. Rev. B 25, 755 (1982).
[19]R. W. Strayer, W. Mackie, and L. W. Swanson, Surf. Sci. 34, 225 (1973); T. V. Vorburger, D. Penn, and E. W. Plummer, *ibid.* 48, 417 (1975).
[20]See, for example, P. J. Jennings and S. M. Thurgate, Surf. Sci. 104, L210 (1981).
[21]A. Adnot and J. D. Carette, Phys. Rev. Lett. 38, 1084 (1977).
[22]E. G. McRae, D. T. Pierce, G.-C. Wang, and R. J. Celotta, Phys. Rev. B 24, 4230 (1981).
[23]E. G. McRae and C. W. Caldwell, Surf. Sci. 57, 766 (1976).
[24]J. M. Baribeau, J. D. Carette, P. J. Jennings, and R. O. Jones (unpublished).